Numerical Investigation of a Supercritical CO_2 Centrifugal Compressor with an In-House Density Based Compressible CFD Solver

Renan Emre Karaefe[1(✉)], Pascal Post[1], Marwick Sembritzky[1], Andreas Schramm[1], Francesca di Mare[1], Matthias Kunick[2], and Uwe Gampe[3]

[1] Ruhr University Bochum, Faculty of Mechanical Engineering, Chair of Thermal Turbomachines and Aeroengines, 44780 Bochum, Germany
{emre.karaefe,pascal.post,marwick.sembritzky,andreas.schramm, francesca.dimare}@rub.de

[2] Zittau/Goerlitz University of Applied Sciences, Faculty of Mechanical Engineering, Department of Energy Systems Technology, 02763 Zittau, Germany
m.kunick@hszg.de

[3] Technische Universität Dresden, Faculty of Mechanical Science and Engineering, Chair of Thermal Power Machinery and Plants, 01062 Dresden, Germany
uwe.gampe@tu-dresden.de

Abstract. This work presents a numerical investigation of the performance characteristics, flow field and internal aerodynamic losses of a supercritical CO_2 centrifugal compressor. The investigated compressor geometry is deduced from main dimensions of a sCO_2 test-loop main compressor operated by Sandia National Laboratories. Three-dimensional CFD simulations are performed with an in-house hybrid CPU/GPU compressible CFD solver. An efficient and accurate real gas property tabulation technique, the Spline-Based Table Look-Up Method (SBTL), which is particularly optimised for the densitiy based solution method, is coupled to the flow solver to account for thermophysical properties. CFD simulations are compared to experimental data as well as a 1D-meanline analysis.

Keywords: sCO_2 · Centrifugal compressor performance · Real gas CFD and property tabulation · 1D-meanline analysis

1 Introduction

Recently, supercritical CO_2 Brayton cycles have gained increasing attention due to their comparatively high thermal efficiency (≈38–50%) at moderate cycle temperatures (450–600 °C) [1]. This is possible because significantly less compression work is required when compressors are operated near the critical point with high fluid density. A high fluid density also allows for a compact turbomachinery design and an overall small footprint of the respective cycle.

M. Pini et al. (Eds.): NICFD 2020, ERCOFTAC Series 28, pp. 87–99, 2021.
https://doi.org/10.1007/978-3-030-69306-0_10

Besides stable process control and compact heat exchanger design, satisfactory turbomachinery performance levels leave room for cycle improvements. Although centrifugal compressor design and analysis is sophisticated for fluids which show ideal gas behaviour, the applicability of respective methods for real fluids showing non-linear behaviour, especially in near-critical state, is uncertain. In this regard, high fidelity CFD simulations, with an accurate thermophysical property representation, allow for detailed insight into the flow field and promise to be an effective tool to improve aerodynamic design and analysis.

The most accurate equation of state for CO_2 is given by Span & Wagner (SW-EOS) [29] and is predominantly integrated into numerical simulations of sCO_2 compressors through lookup tables, due to its high computational overhead. Most noticeably, a sCO_2 main compressor installed in a compression test-loop operated by Sandia National Laboratories (SNL) [32,34] has been investigated through this approach by several researchers. The referenced case is of great interest and also investigated in this work because rare geometrical and experimental data is partially documented. In numerical studies related to the SNL compressor, bilinear interpolation schemes were predominantly applied to compute properties between discrete tabulated values. These require extensive table refinements in order to capture highly non-linear property behaviour. According to Ameli et al. [2,4], such refinements are often the cause for simulation instabilities, which can be coped by a labour-intensive initialisation procedure. In this regard, the applied numerical framework based on the application of biquadratic spline interpolation promises improved simulation stability as well as desirable computing times.

2 Scope of Research

The numerical framework, comprising the in-house CFD solver coupled to the SBTL method, is applied for performance as well as flow field assessments of a centrifugal compressor operating with CO_2. The investigated geometry is deduced from main dimensions of the SNL main compressor, which is designed for operation near the critical point, and has been experimentally investigated by Wright et al. [32,34] and Fuller & Eisemann [12]. Beside a near-critical thermodynamic inlet condition, also a compressor inlet state in the gas phase is considered, where the compressor could potentially be operated during cycle startups. Complementary to the CFD assessments, previously reported in [18], a 1D-meanline analysis is conducted in this study to provide a further reference for performance calculations and to estimate as well as separate the contribution of internal loss mechanisms.

3 Methodology

3.1 Numerical Procedure

The in-house density based compressible CFD solver SharC [25] is applied for all simulations in this study. The Reynolds-averaged Navier-Stokes equations are

solved, which are closed by general thermodynamic state expressions as well as constitutive equations. Governing equations are spatially discretised on structured grids using a finite-volume approach. A central scheme is applied for diffusive flux discretisation, while advective fluxes are discretised through a second order AUSM+ scheme [24] using a piecewise linear MUSCL reconstruction [30]. An implicit LUSGS scheme is utilised for time integration and closure of the RANS-equations is achieved by applying the turbulence model of Spalart & Allmaras [28]. Recent solver applications comprise the topics of non-equilibrium wet steam [25], involving the first LES of a condensing wet steam turbine cascade [26], humid air [14] and sCO_2 [18].

3.2 Real Gas Property Tabulation

Real gas thermodynamic properties of CO_2 based on the SW-EOS as well as thermal conductivity and viscosity are accessible in the solver via a software library integration of the Spline-Based Table Look-Up Method (SBTL), specifically developed for fast and accurate fluid-property computations in extensive numerical simulations [19,20]. The method is based on spline interpolation techniques using lower order polynomials, such as biquadratic or bicubic spline functions. Unlike local bilinear interpolation, biquadratic spline functions provide continuous first derivatives. Furthermore, biquadratic spline functions can be solved quickly with respect to their independent variables. In this way, numerically consistent backward functions can be calculated, which are faster than those obtained from the inversion of bicubic polynomials. Also, simple search algorithms are applicable as the construction of spline functions is performed on piecewise equidistant nodes. The permissible deviations are smaller than the uncertainties of the SW-EOS and the transport property correlations, except for thermal conductivity and isobaric heat capacity, which become infinite at the critical point. Throughout the simulations, thermodynamically stable states are considered only, i.e. fluid properties beyond the saturation curves are calculated as a homogenous equilibrium mixture in the two-phase region.

3.3 Geometry Generation and Computational Setup

The impeller geometry of the SNL compressor is investigated, which is not publicly reported in all details. Therefore, some main dimensions given in [34], along with additional part drawings reported in [32,34], were used to design an impeller with comparable main dimensions. For the sake of simplification, tip clearance was not considered. A 3D geometric model (see Fig. 1a) was generated through fixed inputs to a preliminary design-tool and its corresponding interface to a blade generation module [7,8].

The computational domain (see Fig. 1b) was generated with an automated multi-block structured mesh generator [22]. Because of rotational periodicity, a single blading passage comprising approximately 1.7 million cells (max. expansion ratio $\approx$ 2.6, min. skewness angle $\approx$ 19°) and a near-wall clustering was considered. Constant total temperature and total pressure corresponding to

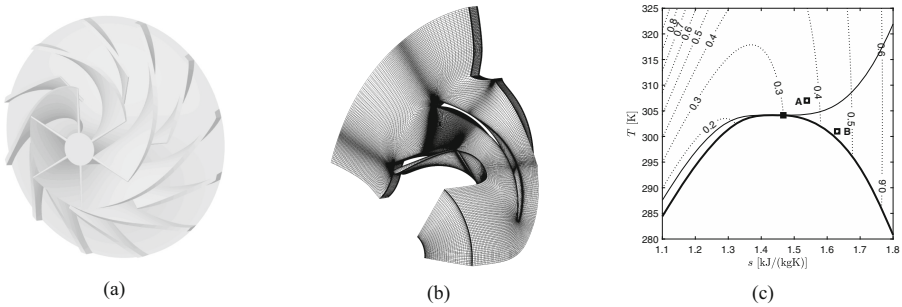

Fig. 1. (a) Impeller wheel geometry, (b) Computational domain, (c) Ts-diagram with markers corresponding to the investigated compressor inlet total states; state A: T_t = 307 K, p_t = 77.5 bar; state B: T_t = 301 K, p_t = 67.9 bar; contour lines show the compressibility factor.

the two investigated inlet states, which are stated and illustrated in Fig. 1c, as well as a turbulent viscosity ratio were imposed at the domain inlet. A constant static pressure was defined as the outlet boundary condition. The imposed outlet static pressure values were (92, 93, 94, 95, 96, 96.5, 96.75) bar to calculate the compressor performance speedline at 50 krpm rotational speed for the near-critical total inlet state (state A). For compressor operation at a total inlet condition in the gas phase (state B), outlet static pressure values of (78, 78.25, 78.5, 79, 80, 81, 81.5, 81.75) bar were specified to derive the 50 krpm performance speedline. The no-slip condition was applied at all walls, which were defined as adiabatic. A routine initialisation procedure was applicable for the RANS calculations, even for simulations with a specified inlet state close to the critical point. The solution domain of the first calculation of each speedline assessment was initialised with spatially linear interpolated values between the domain inlet and outlet for the cyclindrical velocity components as well as pressure and temperature. These were guessed from initial meanline calculations. Consecutive RANS calculations were initialised from the solution of previous converged runs. Compared to ideal gas calculations, which are used as a benchmarking reference, the coupling of the solver to the SBTL library resulted in a computational overhead of merely 33%, providing desirable time-efficiency.

3.4 Meanline Analysis Procedure

In this work, a single-zone modelling approach is applied, which incorporates a loss model set that was suggested by Oh et al. [23] as the most suitable among the possible combinations of most of the loss models in the literature. The loss model set was validated by Oh et al. for a variety of centrifugal compressors operating with working fluids obeying the ideal gas law and also adopted and stated to be valid for the calculation of the SNL sCO_2 main compressor [3,21,27]. For impeller calculations, six sources of internal losses and three sources of external losses are distinguished, which are all expressed in an enthalpy (adiabatic head

loss) formulation and listed in Table 1. External losses, which are also called parasitic losses, differ from internal aerodynamic losses in that they give rise to the impeller stagnation enthalpy, but do not contribute to pressure rise:

$$\Delta h_t = W_{Euler} + \sum W_{external} \overset{\text{here}}{=} W_{Euler} + W_{df} + W_{rc} + W_{lk} \quad \text{(assuming adiabatic flow).} \tag{1}$$

In addition to the loss model set, a slip factor correlation

$$\sigma = 1 - \frac{\sqrt{\cos \beta_{2,bl}}}{Z_{bl}^{0.7}} \qquad \text{(meridional angle system),} \tag{2}$$

based on a formulation given by Wiesner [31] is implemented, which is necessary in order to deduce the actual work input of the impeller blades through the Euler equation, compared to the case where the fluid would be perfectly guided by the blades (e.g. if there were an infinite number of infinitesimally thin blades):

$$W_{Euler} = u_2 c_{2\theta} - u_1 c_{1\theta} = u_2(\sigma u_2 + c_{2m} \tan \beta_{2,bl}) \qquad \text{(meridional angle system).} \tag{3}$$

The meanline analysis procedure is implemented in PYTHON and accounts for the thermophysical properties of sCO_2 by direct calls to the open-source property library CoolProp [6]. In addition, an ideal gas calculation procedure is available, that is suitable for performance calculations of centrifugal compressor impellers operating with conventional working fluids, which obey the ideal gas equation. A sample validation example for performance prediction capabilities of the latter is presented in Fig. 2, based on the well documented NASA LSCC air compressor impeller test case [13].

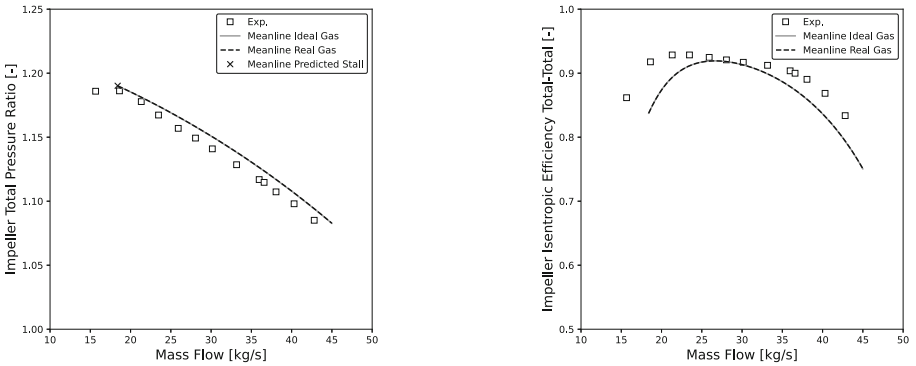

Fig. 2. Meanline performance analysis of the NASA LSCC air centrifugal impeller [13] conducted for design rotational speed on the basis of the real gas and the ideal gas calculation routine. The stall indication criterion is taken from [5].

Table 1. Set of internal and external (parasitic) loss models

Loss mechanism	Loss model		Reference
Incidence	$\Delta h_{inc} = \sigma \cdot \frac{\left(w_{1\theta} - w_{1\theta,bl}\right)^2}{2}$	$\sigma = 0.5...0.7$	Conrad et al. [9]
Blade loading	$\Delta h_{bl} = 0.05 \cdot D_f^2 \cdot u_2^2$	$D_f = 1 - \frac{w_2}{w_{1t}} + \frac{0.75 \cdot W_{Euler}/u_2^2}{w_{1t}/w_2\left[\frac{Z_{bl}}{\pi}\left(1-\frac{d_{1t}}{d_2}\right)+2\frac{d_{1t}}{d_2}\right]}$	Coppage et al. [10]
Skin friction	$\Delta h_{sf} = 2c_f \frac{L_{fl}}{d_{hb}} \bar{w}^2$	$\bar{w} = \frac{(2w_2 + w_{1t} - w_{1h})}{4}$	Jansen [15]
		$L_{fl} \approx \frac{\pi}{8}\left(d_2 - \frac{d_{1t}+d_{1n}}{2} - b_2 + 2L_{ax}\right)\left(\frac{2}{\frac{\cos\beta_{1t}+\cos\beta_{1h}}{2}+\cos\beta_2}\right)$	
		$d_{hb} = \frac{d_2\cos\beta_2}{\frac{Z_{bl}}{\pi}+\frac{d_2\cos\beta_2}{b_2}} + \frac{\frac{d_2}{2}\left(\frac{d_{1t}}{d_2}+\frac{d_{1h}}{d_2}\right)\left(\frac{\cos\beta_{1t}+\cos\beta_{1h}}{2}\right)}{\frac{Z_{bl}}{\pi}+\left(\frac{d_{1t}+d_{1n}}{d_{1t}-d_{1n}}\right)\left(\frac{\cos\beta_{1t}+\cos\beta_{1h}}{2}\right)}$	
		$c_f = 0.0412Re^{-0.1925};\ Re = \frac{d_{hb}\bar{w}}{\nu}$	
Clearance	$\Delta h_{cl} = u_2^2 0.6\frac{\delta}{b_2}\frac{c_{2\theta}}{u_2} \times\sqrt{\frac{4\pi}{b_2 Z_{bl}}\left[\frac{r_{1t}^2 - r_{1h}^2}{(r_2 - r_{1t})(1+\rho_2/\rho_1)}\right]\frac{c_{2\theta}}{u_2}\frac{c_{1m}}{u_2}}$		Jansen [15]
Mixing	$\Delta h_{mix} = \frac{1}{2}\frac{c_2^2}{1+(c_{2\theta}/c_{2m})^2}\cdot\left[\frac{1-\epsilon-B}{1-\epsilon}\right]^2$		Johnston & Dean [17]
Disk friction	$W_{df} = f_{df}\frac{\bar{\rho} r_2^2 u_2^3}{4\dot{m}}$	$\bar{\rho} = \frac{\rho_1+\rho_2}{2};\quad f_{df} = \begin{cases} \frac{2.67}{Re_{df}^{0.5}}, & Re_{df} < 3\cdot 10^5 \\ \frac{0.0622}{Re_{df}^{0.2}}, & Re_{df} \geq 3\cdot 10^5 \end{cases}$	Daily & Nece [11] as quoted by Oh et al. [23]
Recirculation	$W_{rc} = 8\cdot 10^{-5}\sinh\left(3.5\alpha_2^3\right) D_f^2 u_2^2$		Oh et al. [23]
Leakage	$W_{lk} = \frac{\dot{m}_{cl} u_{cl} u_2}{2\dot{m}}$	$u_{cl} = 0.816\sqrt{2\Delta p_{cl}/\rho_2};\ \dot{m}_{cl} = \rho_2 Z_{bl}\delta L_{fl} u_{cl}$	Aungier [5]
		$\Delta p_{cl} = \frac{\dot{m}(r_2 c_{2\theta} - r_1 c_{1\theta})}{Z_{bl}\bar{r}\bar{b}L_{fl}};\ \bar{r} = \frac{r_1+r_2}{2};\ \bar{b} = \frac{b_1+b_2}{2}$	

Note: Equations are presented for the meridional angle convention. The nomenclature is given in SI units. B: ratio of diffuser inlet depth to impeller tip flow passage depth, b: width, c: absolute velocity, d: diameter, h: specific enthalpy, L_{ax}: axial length of impeller, $\dot{m}$: mass flow, r: radius, u: peripheral velocity, W: specific work, w: relative velocity, Z_{bl}: number of blades, α: absolute flow angle, β: relative flow angle, δ: clearance gap width, ϵ: fraction of blade-to-blade space occupied by the wake, η: dynamic viscosity, ν: kinematic viscosity, ρ: density, $(\circ)_1$: impeller inlet, $(\circ)_2$: impeller exit, $(\circ)_{bl}$: blading, $(\circ)_h$: hub, $(\circ)_m$: meridional, $(\circ)_t$: tip, $(\circ)_\theta$: tangential

4 Results

4.1 Performance Analysis

Results of the RANS-based performance calculations, previously reported in [18], and the meanline analysis for the two distinct inlet states are compared to the available experimental data reported by Wright et al. [32,34] and Fuller & Eisemann [12] in Fig. 3. The experimental performance data is interpreted to be associated with the impeller wheel, based on the instrumentation reported in [32,34] (static pressure tap at the impeller wheel exit) and the statement given in [32] that impeller wheel efficiencies (given as isentropic total-to-static efficiencies) were predicted through meanline codes and compared to experimental data. Because of high fluctuations in inlet conditions, the experimental data is provided in corrected and non-dimensionalised form. Consequently, a non-dimensionalised representation is adopted for the sake of comparison through

the impeller ideal head coefficient $\psi = {}^{(h_{2s}-h_{t1})}/_{u_2^2}$ and the impeller total-to-static isentropic efficiency $\eta_s = {}^{(h_{2s}-h_{t1})}/_{(h_{t2}-h_{t1})}$, both plotted against the flow coefficient $\phi = {}^{4\dot{V}_1}/_{(\pi d_2^2 u_2)}$. Impeller exit values in CFD calculations are derived from a radial plane at $r/r_2 \approx 1.008$. This corresponds to the radial position halfway between the impeller exit radius and the vaned diffuser leading edge radius in the experimental setup.

Compared to the experimental data at the near-critical operating condition (state A), the RANS calculations show an overall flatter characteristic with higher ideal impeller head generation observed for data points at comparatively high flow coefficients and lower head generation than in the experiments towards lower flow coefficients. Noticeably, both experimental data sets share a similar qualitative shape. However, a reduced operating margin towards surge can be identified in the data set provided by Fuller & Eisemann. Since the experiments were performed with a channel diffuser, which generally restricts the flow range compared to a vaneless configuration, the flow range between experiment and CFD is not directly comparable. Range assessments are also omitted in the meanline analysis, which is presented for a setup with and without the consideration of tip clearance. Note that external (parasitic) losses are excluded in the meanline analysis for better comparability with the RANS simulations, where these are not assessed, and the experiments. For the latter, electric, magnetic and mechanical power losses estimated through correlations were excluded from the efficiency calculations, which were based on motor power measurements [32,33].

As a relatively high sensitivity towards input of the parameter ϵ was identified, which defines the fraction of blade-to-blade space occupied by the wake in the mixing loss model of Johnston & Dean [17], it is varied for three sample values for the case without tip clearance. A value of $\epsilon = 0.45$ is considered to be the most common assumption for centrifugal compressors (based on the common value of 0.2 for the wake mass fraction χ and the model formulation $\chi = \epsilon^2$, both reported in [16]) and leads to a good qualitative agreement with the RANS calculations concerning efficiency. However, in case of the head curve, a reduced value of $\epsilon = 0.35$ leads to better and satisfactory qualitative as well as quantitative agreement with the RANS calculations. The registered peak efficiency in the RANS calculations is approximately 54.4% and more than ten percentage points lower than the highest values of the highly scattered experimental data. Meanline efficiency predictions with $\epsilon = 0.45$ exceed the RANS assessment by about 5 percentage points. The consideration of tip clearance leads to decrease of 7 to 14% in head generation and a decrease in efficiency of around 4 to 6 percentage points in the meanline analysis, indicating an influential impact on compressor performance.

Comparing the datasets of the performance calculations (RANS and meanline) for the gaseous inlet state (state B) to those of the near-critical inlet state (state A), almost no difference can be observed, evidencing a high degree of machine similarity. The experimental head curve is comparable to those of the near-critical state, but shows a flatter characteristic and therefore, a better agreement between experiment and numerics is derived at this operation state. Overall, considering the high uncertainties of the test case related to the exact

geometry, knowledge of the exact data assessment positions and stable process conditions in experiments, reasonable performance metrics are derived that provide a solid foundation for flow investigations.

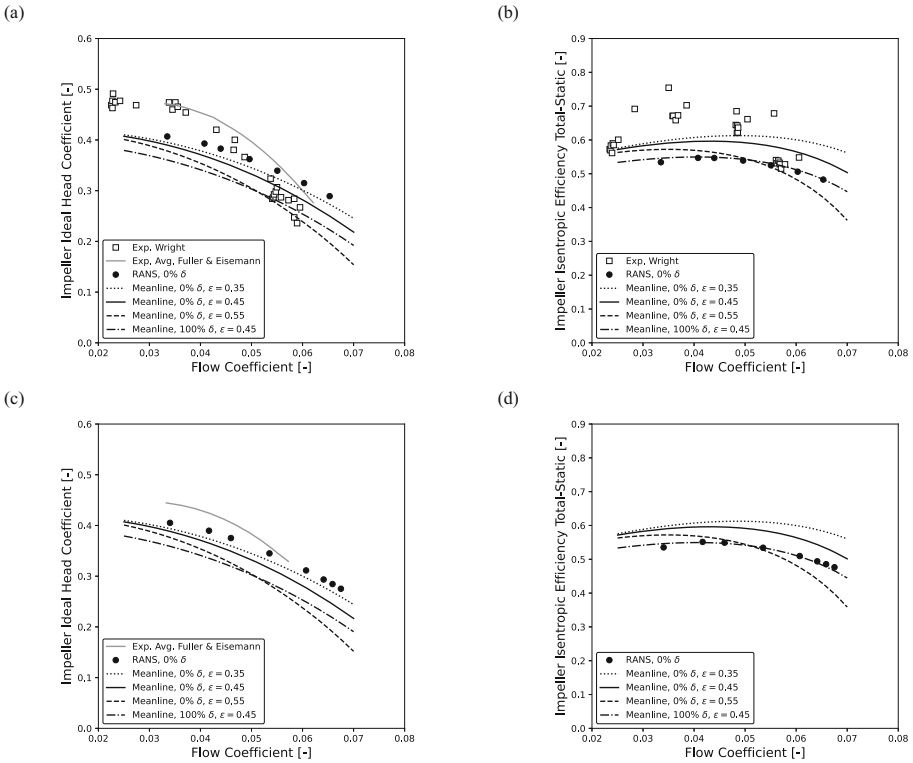

Fig. 3. Impeller performance for the total inlet condition at state A (a, b) and state B (c, d) at 50 krpm rotational speed, compared to experimental data of Wright et al. [32,34] and Fuller & Eisemann [12]. Note: δ: clearance gap width; ϵ: fraction of blade-to-blade space occupied by the wake, see also mixing loss model of Johnston & Dean [17] in Table 1.

4.2 Internal Loss Distribution Within the Meanline Analysis

The share of each considered loss mechanism in the total internal loss calculated within the meanline analysis procedure is assessed for both compressor inlet states and for different flow coefficients in Fig. 4. These calculations were performed with tip clearance and the commonly applied value of $\epsilon = 0.45$. Both charts show an almost identical loss distribution, thus supporting the indication of a high degree of machine similitude, which was illustrated in the non-dimensional performance maps. Across the entire flow spectrum, tip clearance losses are identified as a very dominant loss contributing factor, with shares of

around 40%. This can be attributed to the relatively wide tip clearance gap, compared to the overall scale of the compact sCO_2 machine ($\delta/d_2 \approx 0.007$). Only for comparatively high flow coefficients, the mixing loss exceeds the clearance loss and explains the high sensitivity of the performance curves towards empirical inputs of the spatial wake fraction ϵ in these flow regions. While skin friction losses contribute with a rather constant share of around 10% of the total internal loss, blade loading losses accounting for secondary flow losses due to blade-to-blade pressure gradients are expectedly apparent for the low flow coefficient states, which overall are associated with high pressure gradients within the impeller. Considering incidence losses, it has to be taken into account that the blade angle distribution at the impeller inlet is not fully documented. Inducer blade angles were estimated on basis of the only given blade angle at the inducer tip and velocity triangle relations at design rotational speed (75 krpm), under the assumption of a constant spanwise meridional velocity and no incidence.

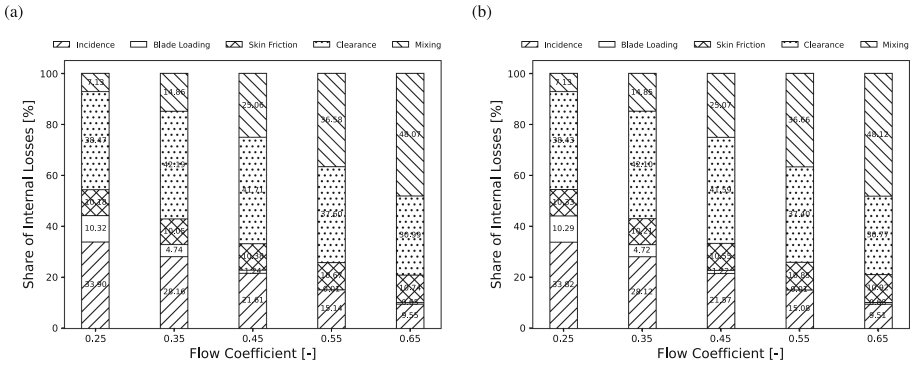

Fig. 4. Share of individual loss mechanisms in the total internal loss for different operating conditions at fixed compressor inlet total conditions at state A (a) and state B (b) at 50 krpm rotational speed.

4.3 Flow Field Analysis

Most noticeably, fluid zones with thermodynamic states within the vapour-liquid region can be identified through flow field analysis, previously reported in [18], for all operating conditions at both of the investigated compressor inlet states (exemplary shown for a single operating point in Fig. 5a). These fluid regions are observed to be located near the impeller blade leading edges and at their suction side (see Fig. 5b), where flow acceleration (see Fig. 5c) yields decreased static conditions. Volume fractions of vapour-liquid fluid regions as part of the entire computational domain were quantified for different flow coefficients and indicated a maximum share below 0.02% for state A and below 1.1% for state B, the latter being expectedly higher due to the closer location to the vapour-liquid region. However, a detailed investigation of the two-phase flow has to account

for metastable states and non-equilibrium condensation of CO_2. This will be subject to extensions of the numerical framework.

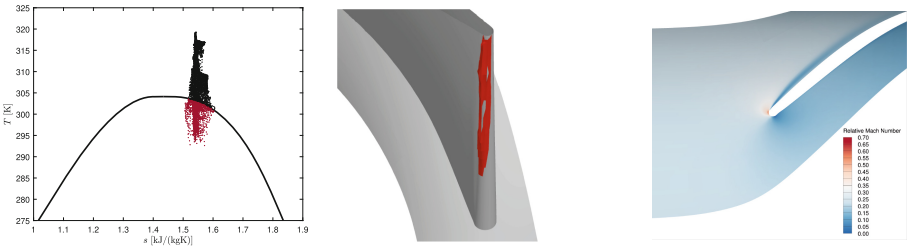

(a) (b) (c)

Fig. 5. Flow field assessments for compressor operation at state A and a flow coefficient of $\phi \approx 0.041$: (a) T,s-diagram with scattered data of the solution domain; (b) Isovolume of data points inside the vapour-liquid two-phase region near the leading edge of the impeller main blade; (c) Contour plot of the relative Mach number distribution near the leading edge of the impeller main blade.

5 Conclusions and Future Works

This work presents a numerical investigation of a supercritical CO_2 centrifugal compressor performed with an in-house CPU/GPU compressible CFD solver and complemented with a 1D single-zone meanline analysis, based on an enthalpy loss formulation. Real gas thermophysical properties within CFD calculations are accounted for by applying the Spline-Based Table Look-Up Method (SBTL), which was particularly developed for time-efficient and accurate fluid-property computations in extensive numerical simulations. Benchmarking the computational speed of the applied methodology against an ideal gas computation indicated a computational overhead of merely 33%. The candidate compressor geometry is based on the geometry of a main compressor installed in a test-loop at Sandia National Laboratories (SNL). Despite the approximation of geometry, which limits quantitative comparison against experimental data, reasonable performance metrics are obtained for compressor operation at an inlet state near the critical point as well as an inlet state in the gas phase, demonstrating the accuracy of the applied methodology. A non-dimensionalised representation of the numerically derived performance parameters shows almost no difference for both investigated compressor operation inlet conditions in comparison, which is an indication for a high degree of machine similitude. Referenced non-dimensional experimental performance data also shows comparability for the two investigated inlet states. These observations suggest that non-dimensionalised sCO_2 compressor performance testing could be numerically and practically conducted at inlet states with less pronounced gradients in thermophysical properties, than observed at operation close to the critical point. Respective findings could then

be related to other inlet states through redimensionalisation. However, it has to be considered that operating states close to the vapour-liquid region might potentially lead to condensation. As a matter of fact, the resolved flow field indicated fluid regions entering the two-phase region, due to flow acceleration near the impeller blade leading edges, for all calculations.

The machine similarity is approved by comparison of the almost identical share of different loss contributing mechanisms on the total internal loss within the meanline analysis, for both inlet states and at varying flow coefficients. It is shown that losses due to tip clearance, which is relatively wide compared to the overall scale of the candidate sCO_2 machine, are a dominant loss contributing factor over the entire operating range. These are only exceeded by mixing losses for high flow coefficients. However, it is identified that the latter are very sensitive to an empirical model input factor accounting for the spatial wake fraction, which limits predictive capabilities.

Overall, the studies within this work prove that the CFD solution method, particularly tailored for the inclusion of real gas tabulation techniques, in combination with SBTL tabulation is a time-efficient and accurate methodology for complex CO_2 real gas computations in the context of turbomachinery. These can be complemented with the presented meanline analysis method considering certain restrictions owed to empirical user input. Future work will focus on integration of metastable states and the assessment of non-equilibrium condensation. Furthermore, the geometry will be extended to account for the channel diffuser in order to improve the prediction capabilities regarding the compressor operating range.

References

1. Ahn, Y., et al.: Review of supercritical CO_2 power cycle technology and current status of research and development. Nucl. Eng. Technol. **47**(6), 647–661 (2015)
2. Ameli, A., Turunen-Saaresti, T., Backman, J.: Numerical investigation of the flow behavior inside a supercritical CO_2 centrifugal compressor. J. Eng. Gas Turbines Power **140**(12), 122604-1–122604-7 (2018)
3. Ameli, A., et al.: Compressor design method in the supercritical CO_2 applications. In: Supercritical CO_2 Power Cycles Symposium, Pittsburgh, Pennsylvania, USA (2018)
4. Ameli, A., et al.: Effects of real gas model accuracy and operating conditions on supercritical CO_2 compressor and flow field. J. Eng. Gas Turbines Power **140**(6), 062603-1–062603-8 (2018)
5. Aungier, R.H.: Mean streamline aerodynamic performance analysis of centrifugal compressors. J. Turbomach. **117**(3), 360–366 (1995)
6. Bell, I., et al.: Pure and pseudo-pure fluid thermophysical property evaluation and the open-source thermophysical property library CoolProp. Ind. Eng. Chem. Res. **53**(6), 2498–2508 (2014)
7. Concepts NREC LLC. AxCent64 (8.7.13.0) (2018)
8. Concepts NREC LLC. COMPAL (8.7.13.0) (2018)

9. Conrad, O., Raif, K., Wessels, M.: The calculation of performance maps for centrifugal compressors with vane-island diffusers. Proceedings of the Twenty-Fifth Annual International Gas Turbine Conference and Exhibit and Twenty-second Annual Fluids Engineering Conference, New Orleans, Louisiana, USA (1979)
10. Coppage, J.E., et al.: Study of supersonic radial compressors for refrigeration and pressurization systems. WADC TECHNICAL REPORT 55-257, Airesearch Manufacturing Company (1956)
11. Daily, J.W., Nece, R.E.: Chamber dimension effects on induced flow and frictional resistance of enclosed rotating disks. J. Basic Eng. **82**(1), 217–230 (1960)
12. Fuller, R.L., Eisemann, K.: Centrifugal compressor off-design performance for super-critical CO_2. In: Supercritical CO_2 Power Cycles Symposium, Boulder, Colorado, USA (2011)
13. Hathaway, M.D., et al.: Laser anemometer measurements of the three-dimensional rotor flow field in the NASA low-speed centrifugal compressor. Army Research Laboratory Technical Report ARL-TR-333, NASA (1995)
14. Iseni, S., Post, P., di Mare, F.: Numerical analysis of the influence of air humidity on a transonic compressor stage. In: International Gas Turbine Congress 2019. Paper No. ThAM16.1, Tokyo (2019)
15. Jansen, W.: A method for calculating the flow in a centrifugal impeller when entropy gradients are present. In: Royal Society Conference on Internal Aerodynamics (Turbomachinery), Cambridge, UK (1967)
16. Japikse, D.: Centrifugal Compressor Design and Performance. Concepts ETI (1996)
17. Johnston, J.P., Dean Jr., R.C.: Losses in vaneless diffusers of centrifugal compressors and pumps: analysis, experiment, and design. J. Eng. Power **88**(1), 49–60 (1966)
18. Karaefe, R.E., et al.: Numerical investigation of a centrifugal compressor for supercritical CO_2 cycles. In: Proceedings of the ASME Turbo Expo 2020. ASME Paper No. GT2020-15194 (2020)
19. Kunick, M.: Fast calculation of thermophysical properties in extensive process simulations with the Spline-Based Table Look-Up Method (SBTL). Fortschritt-Berichte VDI. Nr. 618, Reihe 6, Energietechnik (2018)
20. Kunick, M., et al.: CFD analysis of steam turbines with the IAPWS standard on the Spline-Based Table Look-Up Method (SBTL) for the fast calculation of real fluid properties. In: Proceedings of the ASME Turbo Expo 2015. ASME Paper No. GT2015-43984 (2015)
21. Lee, J., et al.: Design methodology of supercritical CO_2 Brayton cycle turbomachineries. In: Proceedings of the ASME Turbo Expo 2012. ASME Paper No. GT2012-68933 (2012)
22. NUMECA International. AutoGrid5 (13.1) (2018)
23. Oh, H.W., Yoon, E.S., Chung, M.K.: An optimum set of loss models for performance prediction of centrifugal compressors. Proc. Inst. Mech. Eng. Part A J. Power Energy **211**(4), 331–338 (1997)
24. Post, P., di Mare, F.: Highly efficient Euler-Euler approach for condensing steam flows in turbomachines. In: GPPS Montreal 18, Montreal, Canada (2018)
25. Post, P., Sembritzky, M., di Mare.: Towards scale resolving computations of condensing wet steam flows. In: Proceedings of the ASME Turbo Expo 2019. ASME Paper No. GT2019-91269 (2019)
26. Post, P., Winhart, B., di Mare, F.: Large eddy simulation of a condensing wet steam turbine cascade. In: Proceedings of the ASME Turbo Expo 2020. ASME Paper No. GT2020-16064 (2020)

27. Romei, A., et al.: The role of turbomachinery performance in the optimization of supercritical carbon dioxide power systems. J. Turbomach. **142**(7), 071001-1–071001-11 (2020)
28. Spalart, P.R., Allmaras, S.R.: A one-equation turbulence model for aerodynamic flows. In: 30th Aerospace Sciences Meeting and Exhibit, Reno, Nevada, USA (1992)
29. Span, R., Wagner, W.: A new equation of state for carbon dioxide covering the fluid region from the triple-point temperature to 1100 K at pressures up to 800 MPa. J. Phys. Chem. Ref. Data **25**(6), 1509–1596 (1996)
30. van Leer, B.: Towards the ultimate conservative difference scheme. V. A second-order sequel to Godunov's method. J. Comput. Phys. **32**(1), 101–136 (1979)
31. Wiesner, F.J.: A review of slip factors for centrifugal impellers. J. Eng. Gas Turbines Power **89**(4), 558–566 (1967)
32. Wright, S.A., et al.: Supercritical CO_2 compression loop operation and test results. In: Supercritical CO_2 Power Cycles Symposium, Troy, New York, USA (2009)
33. Wright, S.A., et al.: Supercritical CO_2 compression loop operation and test results. Presentation. Supercritical CO_2 Power Cycles Symposium, Troy, New York, USA (2009)
34. Wright, S.A., et al.: Operation and analysis of a supercritical CO_2 Brayton cycle. SANDIA REPORT SAND2010-0171, Sandia National Laboratories (2010)